



HAL
open science

A formin-mediated cell wall- plasma membrane- cytoskeleton continuum is required for symbiotic infections in *Medicago truncatula*

Pengbo Liang, Clara Schmitz, Beatrice Lace, Franck Anicet Ditengou, Jean Keller, Cyril Libourel, Pierre-Marc Delaux, Thomas Ott

► To cite this version:

Pengbo Liang, Clara Schmitz, Beatrice Lace, Franck Anicet Ditengou, Jean Keller, et al.. A formin-mediated cell wall- plasma membrane- cytoskeleton continuum is required for symbiotic infections in *Medicago truncatula*. 2020. hal-02997289

HAL Id: hal-02997289

<https://hal.science/hal-02997289>

Preprint submitted on 10 Nov 2020

HAL is a multi-disciplinary open access archive for the deposit and dissemination of scientific research documents, whether they are published or not. The documents may come from teaching and research institutions in France or abroad, or from public or private research centers.

L'archive ouverte pluridisciplinaire **HAL**, est destinée au dépôt et à la diffusion de documents scientifiques de niveau recherche, publiés ou non, émanant des établissements d'enseignement et de recherche français ou étrangers, des laboratoires publics ou privés.

1 **A formin-mediated cell wall- plasma membrane- cytoskeleton continuum is required for**
2 **symbiotic infections in *Medicago truncatula***

3

4 Short title: The CW-PM-Cytoskeleton continuum during symbiotic infections

5

6 Pengbo Liang ^a, Clara Schmitz ^a, Beatrice Lace ^a, Franck Anicet Ditengou ^a, Jean Keller ^b, Cyril
7 Libourel ^b, Pierre-Marc Delaux ^b, Thomas Ott ^{a,c,*}

8

9 ^a University of Freiburg, Faculty of Biology, Cell Biology, Schänzlestr. 1, 79104 Freiburg,
10 Germany

11 ^b Laboratoire de Recherche en Sciences Végétales (LRSV), Université de Toulouse, CNRS,
12 UPS, Castanet Tolosan, France

13 ^c CIBSS – Centre of Integrative Biological Signalling Studies, University of Freiburg,
14 Germany

15

16 * Correspondence author: Thomas.Ott@biologie.uni-freiburg.de

17

18

19

20 Keywords: Nodulation; symbiosis; actin; rhizobial infection; legume

21 **ABSTRACT**

22 Plant cell infections are tightly orchestrated by cell wall (CW) alterations, plasma membrane
23 (PM) resident signalling processes and dynamic remodelling of the cytoskeleton. During root
24 nodule symbiosis these processes result in morpho-dynamic responses including root hair
25 swelling and curling, PM invagination and polar growth of a tubular infection structure, the
26 infection thread (IT). However, the molecular details driving and guiding these PM
27 remodelling events remain to be unravelled. Here, we studied a formin protein (SYFO1) in *M.*
28 *truncatula* that is specifically induced during rhizobial infection. Phenotypical analysis of *syfo1*
29 mutants clearly indicates that the encoded protein is required for efficient rhizobial colonization
30 of root hairs. SYFO1 itself creates a proteinaceous bridge between the CW and the polarized
31 cytoskeleton. It binds to CW components via a proline-rich N-terminal segment, which is
32 indispensable for its function. On the cytoplasmic side of the PM SYFO1 is associated with
33 actin accumulations supporting the hypothesis that it contributes to cell polarization *in vivo*.
34 This is further sustained by the fact that cell shape changes can be induced in a stimulus-
35 dependent manner in root protoplasts expressing SYFO1. Taken together we provide evidence
36 for the evolutionary re-wiring of a generic cytoskeleton modulator into a symbiosis-specific
37 response.

38
39

40

41 INTRODUCTION

42 Legumes have the unique ability to symbiotically associate with rhizobia to maintain a
43 nitrogen-fixing mutualism. Intracellular colonization of *Medicago truncatula* roots by the
44 compatible rhizobium *Sinorhizobium meliloti* initiates from young, growing root hairs. In the
45 course of the interaction an organogenetic program is executed in the root cortex and the
46 pericycle that results in the development of nodules, in which symbiotic nitrogen fixation takes
47 place [1, 2]. The first morphological step to establish this symbiosis comprises a rhizobial trap,
48 where a growing root hair engulfs the symbiont by physically curling around it [3, 4].
49 Phenomena such as root hair deformation and root hair branching, steps that precede bacterial
50 trapping in legumes [5, 6], have been generally observed in plants in response to the
51 microtubule-stabilizing agent taxol [7], in mutants like the kinesin *mrh2* [8] or upon over-
52 expression of the formin protein AtFH8 [9] and the ROP GTPase RHO-OF PLANTS 2 [10].
53 In contrast, incomplete curls were only observed at low frequency in *Arabidopsis* mutants
54 affected in the loci *CEN1*, *CEN2*, *CEN3* [11] and in the *scn1-1* mutant, where the corresponding
55 locus encodes the RhoGTPase GDP dissociation inhibitor SUPERCENTPEDE1 [12]. This
56 indicates full root hair curling to represent a rather specific invention. The entrapment of the
57 symbiont completes with its full enclosure between root hair cell walls in a structure called the
58 ‘infection chamber’ (IC) [3-5, 13]. This is followed by exocytotic secretion of host-derived cell
59 wall loosening enzymes such as NODULE PECTATE LYASE [14] which, most likely,
60 subsequently allows the formation of a negatively curved plasma membrane (PM) structure
61 that further elongates into a tube-like channel, the ‘infection thread’ (IT) [3, 4, 15]. Parallel to
62 these morphological changes a set of transcription factors genetically re-programs host root
63 cells to allow transcellular IT progression and nodule organogenesis [16-22].
64 Molecularly, initial root hair responses are triggered upon the recognition of bacterial
65 signalling molecules, called Nod Factors, by host LysM-type receptor-like kinases [23-28].

66 These include root hair swelling, deformation and branching that precede root hair curling.
67 This is aided by a tip-localized cytosolic calcium gradient [29, 30], global actin re-
68 arrangements and dense subapical fine actin bundles that are required for the delivery of Golgi-
69 derived vesicles to the root hair tip [5, 31-33]. However, the molecular machinery steering actin
70 reorganisation and polarity during root hair curling remains elusive. Altered actin dynamics
71 during early responses to NFs or rhizobia have been shown in mutants such *Lotus japonicus*
72 *pir1/nap1* and *scarn* that are affected in the actin-related SCAR/WAVE complex [34, 35]. In
73 addition, the presence of highly dynamic F-actin plus ends in swelling root hairs and during
74 root hair deformation implies that newly accumulated actin physically pushes towards the PM
75 to re-initiate the growth [36]. But, different to metazoan cells, where membrane protrusions
76 such as filopodia are driven, among others, by formin-mediated polar growth of actin filaments
77 [37], any membrane protrusions in plant cells ultimately require local cell wall modifications
78 and thus this membrane-cell wall continuum to be coordinatively regulated.
79 Here, we identified SYMBIOTIC FORMIN 1 (SYFO1) as an essential gene controlling
80 symbiotic responses in root hairs. SYFO1 transiently re-localizes to the root hair tip upon
81 inoculation of *M. truncatula* root hairs with *S. meliloti* and mediates the formation of polar
82 actin accumulations. Its function strictly depends on the protein extracellular domain that
83 mediates cell wall attachment. Taken together we demonstrate SYFO1 as the first player
84 regulating the continuum between the plasma membrane and the cell wall during the onset of
85 rhizobial infections.

86 RESULTS

87 Evolutionary and transcriptional patterns identify symbiotically regulated formins

88 Since formins are well known proteins conferring polar growth of actin filaments, we searched
89 for candidates within this family that could control symbiotically induced root hair responses.
90 Based on the presence of a conserved Formin Homology 2 (FH2) domain, we identified 19
91 candidates in the *Medicago truncatula* genome (Table S1). Using publicly available
92 transcriptome data, two of them (*Medtr5g036540.1* and *Medtr8g062830.1*) were found to be
93 transcriptionally up-regulated during early stages of symbiotic interactions [38]. We
94 independently verified these data using quantitative RT-PCR (qRT-PCR) with
95 *Medtr5g036540.1* being induced by about 60-fold at one day post inoculation (dpi) of roots
96 with *S. meliloti* while only a weak induction could be confirmed for *Medtr8g062830.1* at 5 dpi
97 (Fig. S1A). Therefore, we named the genes *SYMBIOTIC FORMIN 1* (*SYFOI*
98 (*Medtr5g036540.1*, *MtrunA17_Chr5g0414941* in the v5r1.6 *M. truncatula* genome version)
99 and SYFO1-like (*SYFOIL*, *Medtr8g062830.1*, *MtrunA17_Chr8g0364331*). Both encoded
100 proteins contain a predicted signal peptide (SP) in the extracellular domain (ECD) followed by
101 a single-span transmembrane domain (TMD), and FH2 domain in the cytoplasmic side.
102 To spatially resolve the observed transcriptional patterns for *SYFOI*, we generated a
103 fluorescent reporter where a nuclear localized tandem GFP was driven by the endogenous
104 *SYFOI* promoter (*ProSYFOI-NLS-2xGFP*). Consistent with the qRT-PCR results (Fig. S1A),
105 the *SYFOI* promoter was activated at 1 dpi in root hairs and cortical cells (Fig.S1 B-C) while
106 no activity was observed in the absence of the symbiont.
107 To supplement the identification strategy and to search for putative genetic redundancy, we
108 studied evolutionary patterns within the formin family. The *SYFOI/IL* clade contains genes
109 from all Eudicots species included in the analysis, and *SYFOI* and *SYFOIL* derived from the
110 Papilionoideae duplication. In *A. thaliana*, three co-orthologs of *SYFOI* and *SYFOIL* are found:

111 *AtFH4*, *AtFH7*, *AtFH8* likely deriving from the Brassicaceae triplication (Fig. S2). While
112 *AtFH4* and *AtFH8* resemble a similar protein domain structure compared to *SYFO1* and
113 *SYFO1L*, *AtFH7* has lost the signal peptide and displays an altered TMD domain. Mining the
114 gene expression atlas of other Papilionoideae, we found *SYFO1* (in common bean,
115 Phvul.002G077100.2) or *SYFO1L* (in *Lotus japonicus* Lj0g3v0115049.1) upregulated during
116 nodulation, pinpointing for a potential shared function in nodulation within this clade.
117 Based on the phylogeny, we tested for relaxed or intensified selective pressure acting on
118 different branches of interest in eudicot sequences (represented by circles) (Fig. S2;
119 Supplemental Table S3). We identified relaxed selective pressure indicated by a higher overall
120 ratio of non-synonymous (dN) vs. synonymous (dS) mutations (dN/dS) on the branch
121 supporting the clade that includes all species that develop the root nodule symbiosis (NFN;
122 $K=0.54$, $LRT=85.3$ and $p\text{-val} < 1e-16$). This relaxation was individually confirmed for Fabales
123 (which includes legumes; $K=0.66$, $LRT=18.3$ and $p\text{-val} < 14.1e-09$), Cucurbitales ($K=0.78$,
124 $LRT=25.0$ and $p\text{-val}=5.6e-07$) and Fagales ($K=0.65$, $LRT=18.3$ and $p\text{-val} < 1.9e-05$) but not
125 for Rosales ($K=1.17$, $LRT=7.4$ and $p\text{-val} < 6.7e-03$) for which a slight intensification of
126 selective pressure (lower overall dN/dS ratio) was detected. In contrast, Brassicaceae species
127 are under strong intensification of the selective pressure ($K=4.6$, $LRT=84.5$ and $p\text{-val} < 1e-16$)
128 that is not even relaxed by the triplication of the branch in this family. The relaxed selection
129 pressure detected at the base of the NFN clade and at the base of the Fabales may both reflect
130 neofunctionalization that would have occurred for the recruitment of *SYFO1/1L* in root nodule
131 symbiosis. Interestingly, the corresponding orthologs of *Parasponia andersonii*, a non-legume
132 tree that forms a Frankia-type symbiosis with rhizobia, are not induced during the symbiotic
133 interaction. This further supports a possible functional specialisation of these forms in
134 legumes /Papilionoideae [39].

135

136 **SYFO1 controls rhizobial infection and root hair responses**

137 In order to genetically assess the function of SYFO1 and SYFO1L, we identified two
138 independent *Tnt1* transposon insertion lines for *SYFO1* [*syfo1-1* (NF9730) at 485bp and *syfo1-*
139 *2* (NF9495) at 1834bp downstream of the start codon] and *SYFO1L* [*syfo1L-1* (NF20350) at
140 1279bp and *syfo1L-2* (NF15608) at 1370bp downstream of the start codon] in Medicago wild
141 type R108 (Fig. 1A). Endogenous *SYFO1* and *SYFO1L* transcripts were significantly reduced
142 in both lines, respectively (Fig. S3), while only the *syfo1-1* and *syfo1-2* alleles showed a
143 significant nodulation phenotype developing fewer nodules per root at 3 weeks post inoculation
144 (wpi) with about half of them being aborted and/or white, indicative of non-functional nodules
145 (Fig. 1B-D). In contrast, bacterial infection patterns of Medicago wild-type and *syfo1L-1* and
146 *syfo1L-2* mutant nodules were identical (Fig. 1C, D and Fig. S4A, B). The infection zones were
147 found to be reduced in white but elongated (Fig. S4C) or spherical (Fig. S4D) *syfo1* mutant
148 nodules. The latter failed to maintain a persistent meristem (Fig. S4D). Therefore, we selected
149 SYFO1 as the prime candidate of interest.

150 Although cytoskeleton-related mutants, like Lotus *pir1*, *nap1* and *scarn* [34, 35], exhibit an
151 impaired root hair growth, this was not observed for *syfo1-1* and *syfo1-2* where root hair length
152 was indistinguishable from wild-type (Fig. S5). In agreement with this, we did not observe any
153 differences in actin arrangement in growing root hairs within the symbiotically susceptible
154 infection zone [4] under non-inoculated conditions (Fig. S6). These data demonstrate that
155 SYFO1 is not required for normal root hair development under non-symbiotic conditions. As
156 *SYFO1* transcripts were upregulated at 1-3 dpi, a stage where we observe most root hairs
157 responding to the presence of the symbiont by root hair deformation (1-2 dpi) (Fig. 2A) and
158 curling (2-3 dpi) (Fig. 2B), we phenotypically assessed *syfo1* mutants at these stages. Both
159 mutant alleles showed significantly fewer deformations (Fig. 2C) as well as infection chambers
160 and infection threads (Fig. 2E) at the respective time points. Both phenotypes were fully

161 rescued when generating independent transgenic roots expressing a *ProSYFO1:SYFO1-GFP*
162 (e.g. *syfo1-1c*) construct in these mutant backgrounds (Fig. 2D, F), demonstrating that the
163 insertion in the *SYFO1* locus is causative for these phenotypes.

164 As it was previously demonstrated that the inoculation of Lotus root hairs with its symbiont *M.*
165 *loti* resulted in a strong polarization and bundling of actin filaments with a strong accumulation
166 of F-actin in the root hair tip [34, 35], we tested whether this pattern is affected in *syfo1* mutants.
167 In the absence of *S. meliloti*, longitudinal actin filaments were observed in young growing root
168 hairs within the infection zone of Medicago wild-type plants (Fig. S7A). In agreement with the
169 observations in Lotus, actin strongly bundled and polarized with an accumulation of F-actin at
170 the apex (Fig. S7B-C) or occasionally at the apical shank of responding root hairs (Fig. S7D)
171 in almost 90% of all root systems of wild-type plants (Fig. S7E). However, this pattern was
172 strongly reduced in both *syfo1* mutant alleles where only about 30% of all tested roots contained
173 root hairs responding with the above-mentioned pattern (Fig. S7E).

174

175 **SYFO1 associates with polar actin assemblies under symbiotic conditions**

176 Since our data indicated a symbiosis-specific role of SYFO1 in root hair polarization, we
177 investigated spatial and temporal dynamics of SYFO1 at subcellular resolution. In roots
178 expressing the *ProSYFO1:SYFO1-GFP* construct, we observed a weak homogenous signal of
179 the SYFO1 protein at the PM of root hairs in the absence of rhizobia (Fig. 3A). The underlying
180 low, basal expression was also detected by qRT-PCR (Fig. S3A) while it was most likely too
181 weak when using the nuclear-localized GFP reporter to test promoter activity (Fig. S1).
182 Interestingly, SYFO1 strongly accumulated in subapical and apical foci at root hair tips prior
183 to deformation at 2 dpi with *S. meliloti* (Fig. 3B, C), which strongly resembled actin patterns
184 observed upon Nod Factor application as reported earlier [34]. In root hairs that
185 morphologically responded by deformation (Fig. 3D) and curling (Fig. 3E), SYFO1 distributed

186 again along the PM with only mild accumulations at the apical region (Fig. 3D). SYFO1 also
187 resided along the infection thread membrane even though to a much weaker extent (Fig. 3F-
188 F'). When co-localizing actin and SYFO1 (here: *ProUbi-SYFO1-GFP*) we frequently observed
189 transient SYFO1 accumulations in close proximity to enlarged nuclei, a hallmark for
190 symbiotically activated root hairs [40], with actin bundles orienting towards a nucleation centre
191 at the apical shank of the root hair (Fig. 3G-G').

192

193 **Ligand-dependent morphological change mediated by SYFO1**

194 To test whether SYFO1 acts in membrane-associated actin nucleation and polar filament
195 elongation, we made use of the fact that extension of actin filaments can drive membrane
196 protrusions as shown in cells lacking a rigid cell wall such as *Drosophila* Schneider 2 and
197 mouse P19 cells [41, 42]. For this, we generated a transgenic *Medicago* root organ culture
198 (ROC) constitutively expressing SYFO1-GFP for 8 weeks. When isolating protoplasts from
199 this culture, SYFO1 resided in the PM where it co-localized with the membrane stain FM4-64
200 with some accumulations in the sub-membrane space (Fig. 3H-H'). While no membrane
201 protrusions were formed in the absence of bacteria, we observed these membrane outgrowths
202 upon inoculation of protoplasts with *S. meliloti* for 5 hours. They coincided with SYFO1
203 accumulations inside these structures and often formed adjacent to bacterial aggregates (Fig.
204 3I-I'). To unambiguously verify that SYFO1 is the key driver of these protrusions we isolated
205 protoplasts from our *syfo1-1* and *syfo1L-1* mutants. No protrusions were found in the absence
206 of rhizobia in any of the used genotypes. Upon inoculation of protoplasts with *S. meliloti*, those
207 expressing wild-type *SYFO1* (wild-type, *syfo1L-1*) or over-expressing SYFO1-GFP (OE)
208 developed protrusions while they were entirely absent on protoplasts isolated from the *syfo1-1*
209 mutant (Fig. 3J). This demonstrates that focal accumulation of SYFO1 can drive cell
210 polarisation and membrane deformations in a stimulus-dependent manner.

211 **A SYFO1-mediated cell wall-plasma membrane-cytoskeleton continuum is required for**
212 **sybiotic responses in root hairs.**

213 As actin binding of formins is generally mediated by the FH2 domain that is also present in the
214 cytosolic domain of SYFO1 (Fig. 1A'), we examined the extracellular region, which is less
215 prominently found among formin proteins. Further sequence analysis of the SYFO1^{ECD}
216 (extracellular domain) revealed the presence of a proline-rich repeat (PRR) (e.g. Ser-Pro-Pro-
217 Pro-Ser-Pro-Ser-Ser [SPPSPSS]) between SP and TMD, which resembles a canonical motif
218 of extensin proteins that have been proposed to contribute to cell wall architecture and tensile
219 strength [43, 44]. Thus we investigated a possible role in cell wall association of the ECD. For
220 this, we fused the 82 amino acids of the SYFO1 ECD to GFP (SYFO1^{ECD}-GFP) and expressed
221 it in *Nicotiana benthamiana* leaf epidermal cells. The fluorescent label was found in the cell
222 periphery in control cells (Fig. 4A-A'') while it remained predominantly associated with the
223 cell wall upon plasmolysis (Fig. 4B-B''). In order to test whether this extensin-like motif
224 contributes to the lateral immobilization of SYFO1 via cell wall anchoring we performed
225 Fluorescence Recovery After Photobleaching (FRAP) experiments on root hairs constitutively
226 expressing a full-length SYFO1 (SYFO1-GFP) or a mutant variant where we deleted the
227 proline-rich repeat (SYFO1^{ΔPRR}-GFP). These experiments revealed a slow recovery of the
228 bleached region and a mobile fraction of about 24% for wild-type SYFO1 whereas the mobile
229 fraction for SYFO1^{ΔPRR} was significantly higher (57%) (Fig. 4C-E). This clearly indicates that
230 the PRR segment within the SYFO1 ECD anchors this formin to the cell wall. To address
231 whether the cell wall association is required for SYFO1 function we conducted genetic
232 complementation experiments, we generated transgenic roots expressing SYFO1^{ΔPRR} under the
233 control of the native *SYFO1* promoter in our *syfo1-1* and *syfo1-2* alleles. In contrast to the full-
234 length SYFO1 (Fig. 2), the deletion of the PRR fully abolished the ability to complement the
235 root hair deformation phenotype of *syfo1* mutants (Fig. 4F), demonstrating that a SYFO1-

236 mediated cell wall-plasma membrane-actin continuum is required for symbiotic responsiveness
237 of root hairs in *M. truncatula*.

238

239 **DISCUSSION**

240 The engulfment of a single rhizobium by a tightly curled root hair represents a fascinating
241 process that allows most legumes to keep full control over the onset of root hair infection and
242 might minimize the risk of infection by non-symbiotic bacteria. Considering that the formin
243 protein SYFO1 serves symbiotic but not general functions in root hair responsiveness (Fig. S5
244 and Fig. S6) demonstrates that *Medicago* genetically re-wired few components of the actin
245 machinery to drive root hair curling. However, the generic set of actin and polarity factors such
246 as NAP1/PIR1, members of the SCAR/WAVE complex [34], and RHO OF PLANTS 10 [45]
247 are additionally required for root hair growth *per se*. Consequently, these mutants show
248 impaired growth also under non-symbiotic conditions. In contrast, legumes specifically
249 evolved SCARN, another member of the SCAR/WAVE complex, which is required for
250 rhizobial infection but not for growth under fully fertilized conditions [35]. The fact that the
251 number of infection chambers was higher in *Lotus scarn* mutants compared to wild-type plants
252 [35], places SCARN downstream of SYFO1. Since the bacterial colonization phenotypes in
253 nodules are comparable between both mutants, both may contribute to actin function at this
254 stage.

255 SYFO1 with its transmembrane helix and the extracellular proline-rich repeat carries all
256 features of a group 1 formin [46]. As previously described for AtFH1 [47], the PRR mediates
257 cell wall association and consequently restricts the lateral mobility also in SYFO1 (Fig. 4E).
258 Its ability to initiate membrane protrusions in cell wall-depleted protoplasts further suggests
259 that SYFO1 is involved in actin nucleation and filament elongation (Fig. 3G-G'; Fig. S8). In
260 line with non-symbiotic formins, such as AtFH4 from *Arabidopsis* that re-localizes to infection

261 sites of the powdery mildew fungus *Blumeria graminis* [48], we hypothesize that SYFO1
262 evolved to specifically mediate targeted secretion of cell wall constituents and other cargo
263 material to sustain symbiotic root hair responses including root hair curling and later stages of
264 infection. This entirely depends on the ability of SYFO1 to associate with the cell wall (Fig. 4)
265 where it maintains a cell wall-plasma membrane-cytoskeleton continuum that cannot be
266 functionally complemented by other, non-symbiotic formins that remain being expressed in
267 *syfo1* mutants.
268

269 MATERIALS AND METHODS

270 Plant growths and phenotypical analysis

271 For phenotypical analysis *Medicago truncatula* wild-type R108, *syfo1-1*, *syfo1-2*, *syfo1L-1* and
272 *syfo1L-2* seeds were scarified and sterilized before being sown on 1% agar plates for
273 germination and kept in darkness at 4°C for 3 days for vernalization. Germination was allowed
274 for up to 24 hours at 24°C before transferring the seedlings to plates containing Fahraeus
275 medium [49] for 4 days in the presence of 1 mM nitrate before being transferred to a plate
276 culture system without nitrogen for phenotyping studies. Plants were inoculated with 1ml
277 *Sinorhizobium meliloti* 2011 (mCherry) at an OD₆₀₀ of 0.05 (on plates or open pots with 1:1
278 ratio of vermiculite and sand mixture). Symbiotic responses including root hair deformations,
279 infection chamber formation and IT development were scored 5 dpi of plants with *S. meliloti*
280 on plates. Soil-based nodulation phenotyping samples were harvested and quantified at 3 wpi.
281 Nodules were embedded in 7% Agar and sectioned with a thickness of 60 µm using a vibratome.
282

283 Genotyping of *Tnt1* insertion lines and quantitative Real-Time PCR

284 R0 or R1 seeds of *M. truncatula* R108 *Tnt1* transposon insertion lines were obtained from the
285 Noble Research Institute (OK, USA) and insertions were verified using primers listed in Table
286 S4. Total RNA of control and insertion lines was extracted using a commercial kit (Spectrum™
287 Plant Total RNA Kit, Sigma life science) following the supplier's instructions. An additional
288 DNaseI treatment was performed. Synthesis of cDNA and qRT-PCR were conducted as
289 described earlier [50] using the SuperScriptIII reverse Transcriptase (Invitrogen). All data were
290 normalized to Ct values of the housekeeping gene ubiquitin [51] using primers listed in Table
291 S4.

292

293

294 **Hairy root transformation and inoculation of rhizobia**

295 *M. truncatula* hairy root transformation was performed as previously described [52] using the
296 *Agrobacterium rhizogenes* strain ARqua1. Plants were transferred weekly to fresh plates
297 containing Fahraeus medium (pH 6.0) supplemented with 0.5 mM NH₄NO₃ and followed by 2
298 days of growth on nitrogen-free Fahraeus medium containing 0.1 μM AVG prior to inoculation.
299 Images for localisation studies and root hair phenotyping analyses were taken on plants
300 inoculated for 2 days and 5 days, respectively.

301

302 **Phylogenetic and selective pressure analysis**

303 SYFO1 (Medtr5g036540.1) and SYFO1L (Medtr8g062830.1) protein sequences were used as
304 queries for a tBLASTn v2.8.1+ (10.1186/1471-2105-10-421) search against a database of 101
305 Angiosperms genomes (Table S2, sequences can be downloaded from the SymDB database
306 (10.1038/s41477-020-0613-7): <http://www.polebio.lrsv.ups-tlse.fr/symdb>) with an e-value
307 threshold of 1e-10. Sequences were then aligned using MAFFT v7.407
308 (10.1093/molbev/mst010) with default parameters. The resulting alignment was trimmed using
309 trimAl v1.4 rev22 (10.1093/bioinformatics/btp348) to remove positions containing more than
310 20% of gaps. The cleaned alignment was then subjected to a Maximum Likelihood (ML)
311 analysis using IQ-TREE v1.6.7 (10.1093/molbev/msu300) as described here after. First, the
312 best-fitting evolutionary model was tested using ModelFinder (10.1038/nmeth.4285). Then a
313 ML search was performed using 10,000 replicates of SH-aLRT (10.1093/sysbio/syq010) for
314 testing branches support. The tree was finally visualized and annotated with iTOL v4.4
315 (10.1093/nar/gkw290).

316 Signal peptide and transmembrane domains were predicted from proteins using signal v5.0
317 (10.1038/s41587-019-0036-z) and TMHMM v2.0c (PMID: 9783223G) respectively using
318 default parameters.

319 To look for relaxation ($K < 1$) or intensification ($K > 1$) of selection acting on different lineages
320 of interest in Eudicots (Table S3), we used the RELAX program (10.1093/molbev/msu400).
321 This method calculates different synonymous and non-synonymous substitution rates ($\omega =$
322 dN/dS) using the phylogenetic tree topology for both foreground and background branches.
323 Because (i) the programs used does not accept gaps in codon sequences and (ii) there is a
324 negative correlation between the number of sequences and the number of ungapped positions,
325 we used different numbers of input sequences for RELAX analysis. Protein sequences from
326 SYFO1 and SYFO1L orthologs were aligned using MUSCLE v3.8.382. Short sequences were
327 excluded to maximize sequence number while limiting gapped positions compared to SYFO1
328 and SYFO1L sequences of *Medicago* using a custom R script. We opted for 151 CDS
329 sequences corresponding to 1008 positions (Table S3).

330

331 **Construct design**

332 The constructs used in this study were designed using Golden Gate cloning [53]. 2.5 kb
333 upstream of the SYFO1 start codon were chosen as putative promoter region. A Golden Gate
334 compatible full-length genomic DNA version (Medtr5g036540.1) was synthesized
335 (GENEWIZ, Germany) by removing the *BpiI* and *BsaI* restriction sites via silent mutations.
336 All cloning primers are listed in Table S4. To select transgenic roots a *pUbi:NLS-mCherry* or
337 *pUbi:NLS-2xCerulean* cassette was additionally inserted into the different T-DNAs containing
338 the transgenes of choice as previously described [50]. Level II and level III constructs were
339 assembled based on the principle described earlier [53]. An overview about all designed
340 constructs is provided in Table S5.

341

342

343 **Confocal Laser-Scanning Microscopy and FRAP**

344 For imaging the NLS-GFP reporter module, sectioned nodules, protein localisation and
345 plasmolysis we used a Leica TCS SP8 confocal microscope equipped with a 20x HCX PL APO
346 water immersion lenses (Leica Microsystems, Mannheim, Germany). GFP was excited with a
347 White Light Laser (WLL) at 488 nm and the emission was detected at 500-550 nm. mCherry
348 fluorescence was excited using a WLL at 561nm and emission was detected between 575-630
349 nm. Samples, co-expressing two fluorophores were imaged in sequential mode between frames.
350 FRAP analysis was conducted using a Zeiss LSM 880 Airyscan confocal microscope. For this,
351 the VP (Virtual Pinhole) mode was adapted based on the fluorescence intensity of probe and
352 Airyscan processing was performed using the ZEN (black edition) software package. The
353 bleaching region, reference region and background region were selected at identical size. A
354 pre-bleaching time of 5 seconds was chosen. Bleaching was set to stop upon the intensity
355 dropping to 50% of the initial intensity before fluorescence recovery was recorded for 10
356 minutes. Using the FRAP data process package in ZEN (black version), the mobile fraction
357 was calculated by the following equation (mobile fraction= $I1/IE$), where $I1$ represents the
358 dropped intensity and the IE represents the recovered intensity normalized to the reference
359 intensity.

360

361 **Root organ culture, protoplast extraction, and inoculation**

362 Transgenic Root Organ Culture (ROC) of *M. truncatula* expressing SYFO1-GFP were
363 obtained via hairy root transformation according to [52]. Fully transformed root segments were
364 cut and initially transferred to M-Media plates (Becard & Fortin, 1988) containing Augmentin
365 (Sigma). 1 g of amoxicillin–200 mg of clavulanic acid) (400 mg/L) for two weeks and then
366 subcultured on plates supplemented with 200 mg/L Augmentin for additional two weeks to
367 remove *A. rhizogenes* contamination. Plates were sealed with micropore tape and incubated at

368 24°C in dark. Afterwards, the ROC was transferred to M-media plates without Augmentin to
369 support faster tissue growth. Continuous expression of the transformation marker was
370 monitored throughout the entire experiment.

371 Protoplasts were isolated from ROC by cutting the roots in small pieces of 2-5 mm length and
372 processed as described previously [54]. For inoculation, an *S. meliloti* culture was diluted in
373 W5 solution [54] to an OD₆₀₀ of 0.05 before being added to the protoplasts.

374

375 **Actin phalloidin staining and plasma membrane FM4-64 staining**

376 Phalloidin-based actin staining was performed according to a published protocol [31]. In brief,
377 *Medicago* roots were transferred into Fahraeus medium containing 300 µM MBS (m-
378 maleimidobenzoyl- N-hydroxysuccinimide ester) for 30 minutes to stabilize the actin filaments.
379 The material was then fixed in 2 % formaldehyde in actin-stabilizing buffer (ASB) solution
380 [34]. Phalloidin was added to a final concentration of 16 µM and staining was performed in the
381 dark for 30 minutes. Root-derived protoplasts were submerged in a FM4-64 solution with a
382 final concentration of 20 µM and incubated on ice for 5-10 mins before imaging.

383

384

385 **ACKNOWLEDGEMENTS**

386 This study was supported by the project Engineering Nitrogen Symbiosis for Africa (ENSA)
387 currently supported through a grant to the University of Cambridge by the Bill & Melinda
388 Gates Foundation (OPP1172165) and UK government's Department for International
389 Development (DFID) as well as by the China Scholarship Council (CSC) (grant no.
390 201506350004 to PL). JK, CL and PMD belong to the LRSV, which is part of the TULIP
391 LABEX (ANR-10-LABX-41). We thank the staff of the Life Imaging Center (LIC) in the
392 Center for Biological Systems Analysis (ZBSA) of the Albert-Ludwigs-University of Freiburg
393 for help with their confocal microscopy resources, and the excellent support in image recording.
394 The *Medicago truncatula* plants utilized in this research project, which are jointly owned by
395 the Centre National De La Recherche Scientifique, were obtained from Noble Research
396 Institute, LLC and were created through research funded, in part, by a grant from the National
397 Science Foundation, NSF-0703285. We are grateful to the genotoul bioinformatics platform
398 Toulouse Occitanie (Bioinfo Genotoul, doi: 10.15454/1.5572369328961167E12) for providing
399 computing resources.

400 We would explicitly thank all the members of our team for the fruitful discussions and for
401 providing their individual expertise throughout the course of the project.

402

403 **The authors declare no competing interests.**

404

405 **Author Contributions**

406 Conceptualization, P.L. and T.O.; Investigation, P.L., C.S., B.L., F.A.D., J.K., C.L., P.M.D.
407 and T.O.; Writing –Original Draft, P.L. and T.O.; Writing –Review & Editing, P.L., C.S.,
408 B.L., F.A.D., J.K., C.L., P.M.D. and T.O.; Funding Acquisition, P.L., P.M.D. and T.O.;
409 Supervision, T.O.

410 **REFERENCES**

411

- 412 1. Mylona, P., Pawlowski, K., and Bisseling, T. (1995). Symbiotic Nitrogen-Fixation.
413 *Plant Cell* 7, 869-885.
- 414 2. Oldroyd, G.E.D., and Downie, J.M. (2008). Coordinating nodule morphogenesis with
415 rhizobial infection in legumes. *Annu Rev Plant Biol* 59, 519-546.
- 416 3. Brewin, N.J. (2004). Plant cell wall remodelling in the rhizobium-legume symbiosis.
417 *Crit Rev Plant Sci* 23, 293-316.
- 418 4. Gage, D.J. (2004). Infection and invasion of roots by symbiotic, nitrogen-fixing
419 rhizobia during nodulation of temperate legumes. *Microbiol Mol Biol R* 68, 280-+.
- 420 5. Esseling, J.J., Lhuissier, F.G.P., and Emons, A.M.C. (2003). Nod factor-induced root
421 hair curling: Continuous polar growth towards the point of nod factor application. *Plant*
422 *Physiology* 132, 1982-1988.
- 423 6. Oldroyd, G.E.D., and Downie, J.A. (2004). Calcium, kinases and nodulation signalling
424 in legumes. *Nat Rev Mol Cell Bio* 5, 566-576.
- 425 7. Bibikova, T.N., Blancaflor, E.B., and Gilroy, S. (1999). Microtubules regulate tip
426 growth and orientation in root hairs of *Arabidopsis thaliana*. *Plant Journal* 17, 657-665.
- 427 8. Yang, G.H., Gao, P., Zhang, H., Huang, S.J., and Zheng, Z.L. (2007). A Mutation in
428 MRH2 Kinesin Enhances the Root Hair Tip Growth Defect Caused by Constitutively
429 Activated ROP2 Small GTPase in *Arabidopsis*. *Plos One* 2.
- 430 9. Yi, K., Guo, C., Chen, D., Zhao, B., Yang, B., and Ren, H. (2005). Cloning and
431 functional characterization of a formin-like protein (AtFH8) from *Arabidopsis*. *Plant*
432 *Physiol* 138, 1071-1082.

- 433 10. Jones, M.A., Shen, J.J., Fu, Y., Li, H., Yang, Z.B., and Grierson, C.S. (2002). The
434 *Arabidopsis* Rop2 GTPase is a positive regulator of both root hair initiation and tip
435 growth. *Plant Cell* *14*, 763-776.
- 436 11. Parker, J.S., Cavell, A.C., Dolan, L., Roberts, K., and Grierson, C.S. (2000). Genetic
437 interactions during root hair morphogenesis in *Arabidopsis*. *Plant Cell* *12*, 1961-1974.
- 438 12. Carol, R.J., Takeda, S., Linstead, P., Durrant, M.C., Kakesova, H., Derbyshire, P., Drea,
439 S., Zarsky, V., and Dolan, L. (2005). A RhoGDP dissociation inhibitor spatially
440 regulates growth in root hair cells. *Nature* *438*, 1013-1016.
- 441 13. Fournier, J., Teillet, A., Chabaud, M., Ivanov, S., Genre, A., Limpens, E., de Carvalho-
442 Niebel, F., and Barker, D.G. (2015). Remodeling of the infection chamber before
443 infection thread formation reveals a two-step mechanism for rhizobial entry into the
444 host legume root hair. *Plant Physiology* *167*, 1233-1242.
- 445 14. Xie, F., Murray, J.D., Kim, J., Heckmann, A.B., Edwards, A., Oldroyd, G.E.D., and
446 Downie, A. (2012). Legume pectate lyase required for root infection by rhizobia. *P Natl*
447 *Acad Sci USA* *109*, 633-638.
- 448 15. Gage, D.J., and Margolin, W. (2000). Hanging by a thread: invasion of legume plants
449 by rhizobia. *Curr Opin Microbiol* *3*, 613-617.
- 450 16. Heckmann, A.B., Lombardo, F., Miwa, H., Perry, J.A., Bunnewell, S., Parniske, M.,
451 Wang, T.L., and Downie, J.A. (2006). *Lotus japonicus* nodulation requires two GRAS
452 domain regulators, one of which is functionally conserved in a non-legume. *Plant*
453 *Physiology* *142*, 1739-1750.
- 454 17. Bek, A.S., Sauer, J., Thygesen, M.B., Duus, J.O., Petersen, B.O., Thirup, S., James, E.,
455 Jensen, K.J., Stougaard, J., and Radutoiu, S. (2010). Improved Characterization of Nod
456 Factors and Genetically Based Variation in LysM Receptor Domains Identify Amino

- 457 Acids Expendable for Nod Factor Recognition in Lotus spp. *Molecular Plant-Microbe*
458 *Interactions* 23, 58-66.
- 459 18. Madsen, L.H., Tirichine, L., Jurkiewicz, A., Sullivan, J.T., Heckmann, A.B., Bek, A.S.,
460 Ronson, C.W., James, E.K., and Stougaard, J. (2010). The molecular network
461 governing nodule organogenesis and infection in the model legume *Lotus japonicus*.
462 *Nat Commun* 1, 10.
- 463 19. Cerri, M.R., Wang, Q.H., Stolz, P., Folgmann, J., Frances, L., Katzer, K., Li, X.L.,
464 Heckmann, A.B., Wang, T.L., Downie, J.A., et al. (2017). The ERN1 transcription
465 factor gene is a target of the CCaMK/CYCLOPS complex and controls rhizobial
466 infection in *Lotus japonicus*. *New Phytologist* 215, 323-337.
- 467 20. Kawaharada, Y., James, E.K., Kelly, S., Sandal, N., and Stougaard, J. (2017). The
468 ethylene responsive factor required for nodulation 1 (ERN1) transcription factor is
469 required for infection-thread formation in *Lotus japonicus*. *Molecular plant-microbe*
470 *interactions* 30, 194-204.
- 471 21. Schauser, L., Roussis, A., Stiller, J., and Stougaard, J. (1999). A plant regulator
472 controlling development of symbiotic root nodules. *Nature* 402, 191-195.
- 473 22. Combier, J.P., Frugier, F., de Billy, F., Boualem, A., El-Yahyaoui, F., Moreau, S.,
474 Vernie, T., Ott, T., Gamas, P., Crespi, M., et al. (2006). MtHAP2-1 is a key
475 transcriptional regulator of symbiotic nodule development regulated by microRNA169
476 in *Medicago truncatula*. *Gene Dev* 20, 3084-3088.
- 477 23. Ben Amor, B. (2003). The NFP locus of *Medicago truncatula* controls an early step of
478 Nod factor signal transduction upstream of a rapid calcium flux and root hair
479 deformation (vol 34, pg 495, 2003). *Plant Journal* 35, 140-140.

- 480 24. Limpens, E., Franken, C., Smit, P., Willemse, J., Bisseling, T., and Geurts, R. (2003).
481 LysM domain receptor kinases regulating rhizobial Nod factor-induced infection.
482 *Science* 302, 630-633.
- 483 25. Madsen, E.B., Madsen, L.H., Radutoiu, S., Olbryt, M., Rakwalska, M., Szczyglowski,
484 K., Sato, S., Kaneko, T., Tabata, S., Sandal, N., et al. (2003). A receptor kinase gene of
485 the LysM type is involved in legume perception of rhizobial signals. *Nature* 425, 637-
486 640.
- 487 26. Arrighi, J.F., Barre, A., Ben Amor, B., Bersoult, A., Soriano, L.C., Mirabella, R., de
488 Carvalho-Niebel, F., Journet, E.P., Gherardi, M., Huguet, T., et al. (2007). The
489 *Medicago truncatula* lysine motif-receptor-like kinase gene family includes NFP and
490 new nodule-expressed genes (vol 142, pg 265, 2006). *Plant Physiology* 143, 1078-1078.
- 491 27. Smit, P., Limpens, E., Geurts, R., Fedorova, E., Dolgikh, E., Gough, C., and Bisseling,
492 T. (2007). *Medicago* LYK3, an entry receptor in rhizobial nodulation factor signaling.
493 *Plant Physiology* 145, 183-191.
- 494 28. Radutoiu, S., Madsen, L.H., Madsen, E.B., Felle, H.H., Umehara, Y., Gronlund, M.,
495 Sato, S., Nakamura, Y., Tabata, S., Sandal, N., et al. (2003). Plant recognition of
496 symbiotic bacteria requires two LysM receptor-like kinases. *Nature* 425, 585-592.
- 497 29. de Ruijter, N.C.A., Rook, M.B., Bisseling, T., and Emons, A.M.C. (1998). Lipochito-
498 oligosaccharides re-initiate root hair tip growth in *Vicia sativa* with high calcium and
499 spectrin-like antigen at the tip. *Plant Journal* 13, 341-350.
- 500 30. Cardenas, L., Feijo, J.A., Kunkel, J.G., Sanchez, F., Holdaway-Clarke, T., Hepler, P.K.,
501 and Quinto, C. (1999). Rhizobium Nod factors induce increases in intracellular free
502 calcium and extracellular calcium influxes in bean root hairs. *Plant Journal* 19, 347-
503 352.

- 504 31. Miller, D.D., de Ruijter, N.C.A., Bisseling, T., and Emons, A.M.C. (1999). The role of
505 actin in root hair morphogenesis: studies with lipochito-oligosaccharide as a growth
506 stimulator and cytochalasin as an actin perturbing drug. *Plant Journal* 17, 141-154.
- 507 32. Miller, D.D., Klooster, H.B.L.-t., and Emons, A.M.C. (2000). Lipochito-
508 oligosaccharide nodulation factors stimulate cytoplasmic polarity with longitudinal
509 endoplasmic reticulum and vesicles at the tip in vetch root hairs. *Molecular plant-
510 microbe interactions* 13, 1385-1390.
- 511 33. Zepeda, I., Sanchez-Lopez, R., Kunkel, J.G., Banuelos, L.A., Hernandez-Barrera, A.,
512 Sanchez, F., Quinto, C., and Cardenas, L. (2014). Visualization of Highly Dynamic F-
513 Actin Plus Ends in Growing Phaseolus vulgaris Root Hair Cells and Their Responses
514 to Rhizobium etli Nod Factors. *Plant Cell Physiol* 55, 580-592.
- 515 34. Yokota, K., Fukai, E., Madsen, L.H., Jurkiewicz, A., Rueda, P., Radutoiu, S., Held, M.,
516 Hossain, M.S., Szczyglowski, K., Morieri, G., et al. (2009). Rearrangement of Actin
517 Cytoskeleton Mediates Invasion of Lotus japonicus Roots by Mesorhizobium loti. *Plant
518 Cell* 21, 267-284.
- 519 35. Qiu, L.P., Lin, J.S., Xu, J., Sato, S., Parniske, M., Wang, T.L., Downie, J.A., and Xie,
520 F. (2015). SCARN a Novel Class of SCAR Protein That Is Required for Root-Hair
521 Infection during Legume Nodulation. *Plos Genet* 11.
- 522 36. Zepeda, I., Sanchez-Lopez, R., Kunkel, J.G., Banuelos, L.A., Hernandez-Barrera, A.,
523 Sanchez, F., Quinto, C., and Cardenas, L. (2014). Visualization of highly dynamic F-
524 actin plus ends in growing phaseolus vulgaris root hair cells and their responses to
525 Rhizobium etli nod factors. *Plant Cell Physiol* 55, 580-592.
- 526 37. Yang, C., Czech, L., Gerboth, S., Kojima, S.I., Scita, G., and Svitkina, T. (2007). Novel
527 roles of formin mDia2 in lamellipodia and filopodia formation in motile cells. *Plos
528 Biology* 5, 2624-2645.

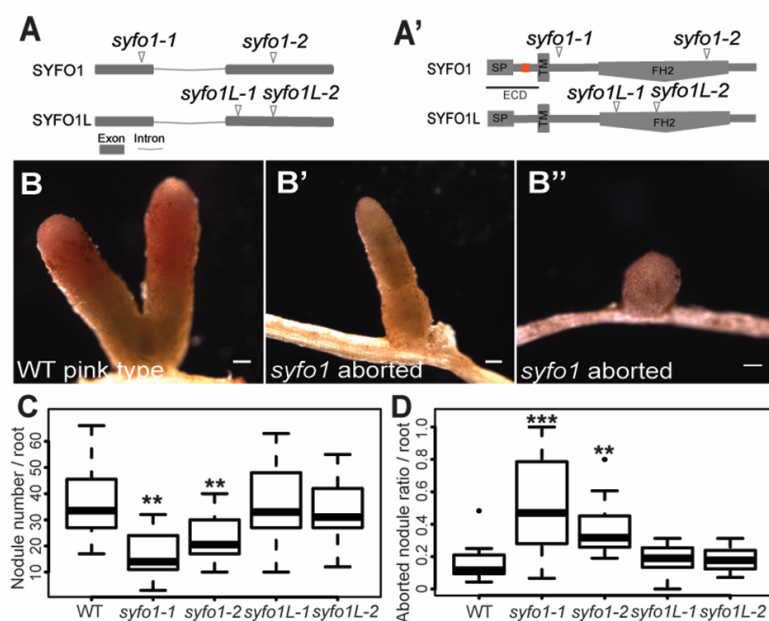
- 529 38. Larrainzar, E., Riely, B.K., Kim, S.C., Carrasquilla-Garcia, N., Yu, H.J., Hwang, H.J.,
530 Oh, M., Kim, G.B., Surendrarao, A.K., Chasman, D., et al. (2015). Deep Sequencing
531 of the *Medicago truncatula* Root Transcriptome Reveals a Massive and Early
532 Interaction between Nodulation Factor and Ethylene Signals. *Plant Physiology* *169*,
533 233-+.
- 534 39. van Velzen, R., Holmer, R., Bu, F.J., Rutten, L., van Zeijl, A., Liu, W., Santuari, L.,
535 Cao, Q.Q., Sharma, T., Shen, D.F., et al. (2018). Comparative genomics of the
536 nonlegume *Parasponia* reveals insights into evolution of nitrogen-fixing rhizobium
537 symbioses. *P Natl Acad Sci USA* *115*, E4700-E4709.
- 538 40. Oldroyd, G.E.D. (2013). Speak, friend, and enter: signalling systems that promote
539 beneficial symbiotic associations in plants. *Nature Reviews Microbiology* *11*, 252-263.
- 540 41. Matusek, T., Gombos, R., Szecsenyi, A., Sanchez-Soriano, N., Czibula, A., Pataki, C.,
541 Gedai, A., Prokop, A., Rasko, I., and Mihaly, J. (2008). Formin proteins of the DAAM
542 subfamily play a role during axon growth. *J Neurosci* *28*, 13310-13319.
- 543 42. Gombos, R., Migh, E., Antal, O., Mukherjee, A., Jenny, A., and Mihaly, J. (2015). The
544 Formin DAAM Functions as Molecular Effector of the Planar Cell Polarity Pathway
545 during Axonal Development in *Drosophila*. *J Neurosci* *35*, 10154-10167.
- 546 43. Estevez, J.M., Kieliszewski, M.J., Khitrov, N., and Somerville, C. (2006).
547 Characterization of synthetic hydroxyproline-rich proteoglycans with arabinogalactan
548 protein and extensin motifs in *Arabidopsis*. *Plant Physiol* *142*, 458-470.
- 549 44. Lamport, D.T., Kieliszewski, M.J., Chen, Y., and Cannon, M.C. (2011). Role of the
550 extensin superfamily in primary cell wall architecture. *Plant Physiol* *156*, 11-19.
- 551 45. Lei, M.J., Wang, Q., Li, X.L., Chen, A.M., Luo, L., Xie, Y.J., Li, G., Luo, D., Mysore,
552 K.S., Wen, J.Q., et al. (2015). The Small GTPase ROP10 of *Medicago truncatula* Is

- 553 Required for Both Tip Growth of Root Hairs and Nod Factor-Induced Root Hair
554 Deformation. *Plant Cell* 27, 806-822.
- 555 46. Deeks, M.J., Hussey, P.J., and Davies, B. (2002). Formins: intermediates in signal-
556 transduction cascades that affect cytoskeletal reorganization. *Trends in Plant Science* 7,
557 492-498.
- 558 47. Martiniere, A., Gayral, P., Hawes, C., and Runions, J. (2011). Building bridges:
559 formin1 of *Arabidopsis* forms a connection between the cell wall and the actin
560 cytoskeleton. *Plant Journal* 66, 354-365.
- 561 48. Sassmann, S., Rodrigues, C., Milne, S.W., Nenninger, A., Allwood, E., Littlejohn, G.R.,
562 Talbot, N.J., Soeller, C., Davies, B., Hussey, P.J., et al. (2018). An Immune-Responsive
563 Cytoskeletal-Plasma Membrane Feedback Loop in Plants. *Curr Biol* 28, 2136-2144
564 e2137.
- 565 49. Fahraeus, G. (1957). The Infection of Clover Root Hairs by Nodule Bacteria Studied
566 by a Simple Glass Slide Technique. *J Gen Microbiol* 16, 374-&.
- 567 50. Liang, P., Stratil, T.F., Popp, C., Marin, M., Folgmann, J., Mysore, K.S., Wen, J., and
568 Ott, T. (2018). Symbiotic root infections in *Medicago truncatula* require remorin-
569 mediated receptor stabilization in membrane nanodomains. *Proc Natl Acad Sci U S A*
570 115, 5289-5294.
- 571 51. Satge, C., Moreau, S., Sallet, E., Lefort, G., Auriac, M.C., Rembliere, C., Cottret, L.,
572 Gallardo, K., Noirot, C., Jardinaud, M.F., et al. (2016). Reprogramming of DNA
573 methylation is critical for nodule development in *Medicago truncatula*. *Nature Plants* 2.
- 574 52. Boisson-Dernier, A., Chabaud, M., Garcia, F., Becard, G., Rosenberg, C., and Barker,
575 D.G. (2001). *Agrobacterium rhizogenes*-transformed roots of *Medicago truncatula* for
576 the study of nitrogen-fixing and endomycorrhizal symbiotic associations. *Mol Plant*
577 *Microbe Interact* 14, 695-700.

- 578 53. Binder, A., Lambert, J., Morbitzer, R., Popp, C., Ott, T., Lahaye, T., and Parniske, M.
579 (2014). A Modular Plasmid Assembly Kit for Multigene Expression, Gene Silencing
580 and Silencing Rescue in Plants. *Plos One* 9.
- 581 54. Jia, N., Zhu, Y.L., and Xie, F. (2018). An Efficient Protocol for Model Legume Root
582 Protoplast Isolation and Transformation. *Frontiers in Plant Science* 9.
- 583
- 584

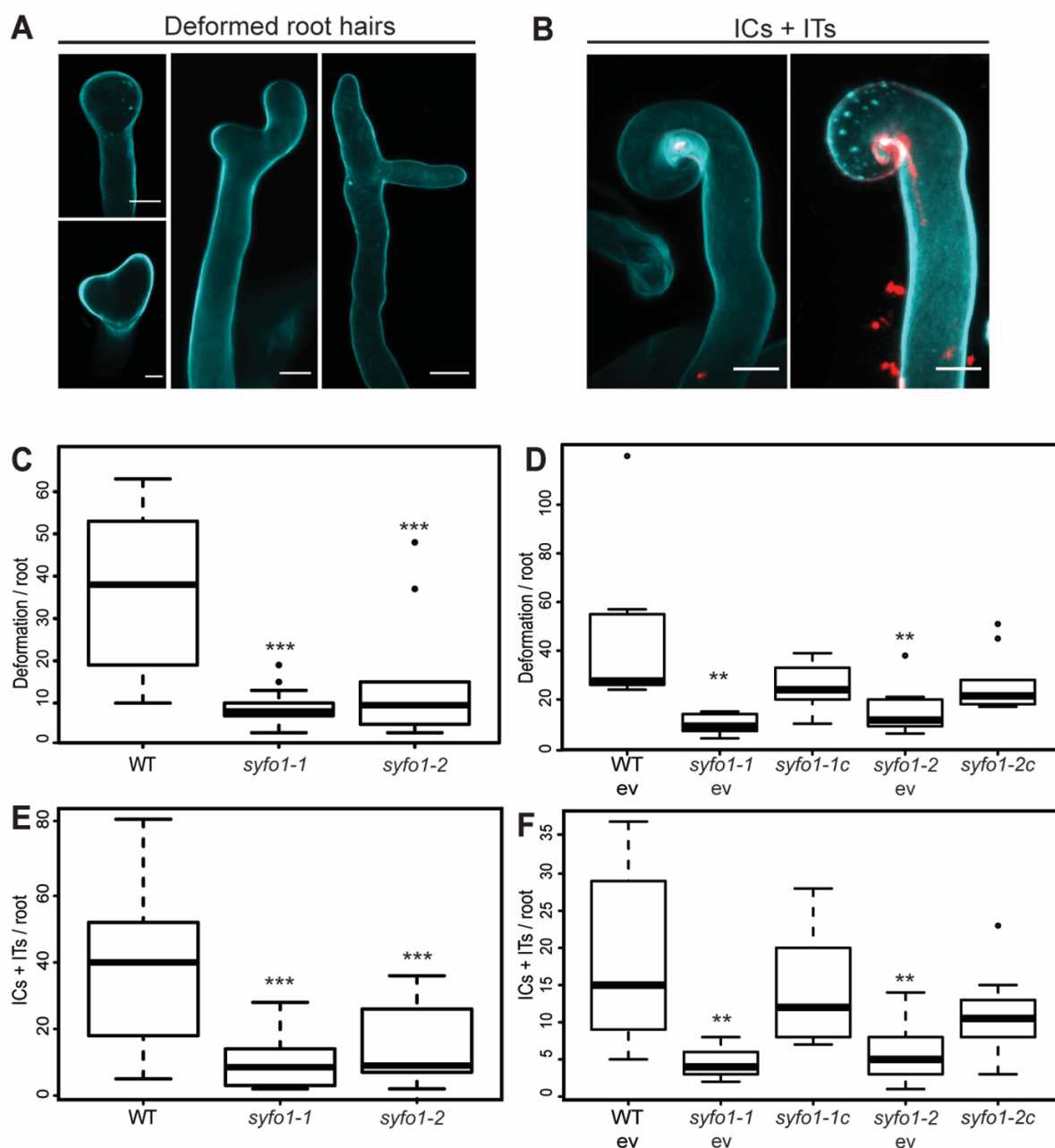
585 **Figures and Legends**

586



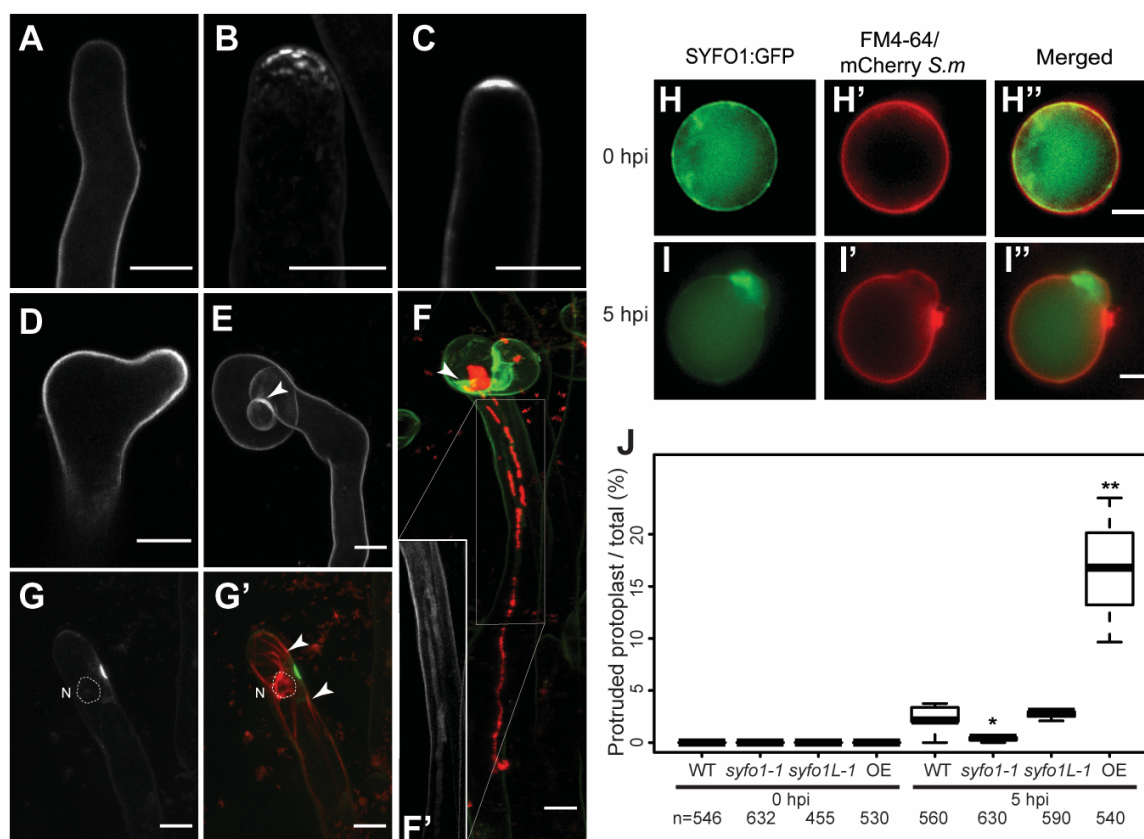
587

588 **Figure 1. SYFO1 but not SYFO1L is required for nodulation.** (A-A') Isolation of independent mutant alleles
 589 with *Tnt1* transposon insertions mapping to different regions of the *SYFO1* and *SYFO1L* gene (A) and protein (A')
 590 models, the extracellular domain is indicated as ECD and the orange box indicated the location of proline-rich
 591 repeat (PRR). (B-B'') Nodule phenotypes observed on the different genotypes at 3 wpi with *S. meliloti* in open
 592 pots using WT R108 plants as a control. Scale bars indicate 200 μm. (C-D) Quantification of nodule numbers (C)
 593 and the ratio of aborted/wild-type like nodules (D) (n=10). Asterisks indicate a significant statistical difference
 594 based on a Tukey–Kramer multiple-comparison test with p-values <0.01 (**), < 0.001 (***). Data are shown as
 595 mean ± SE.
 596



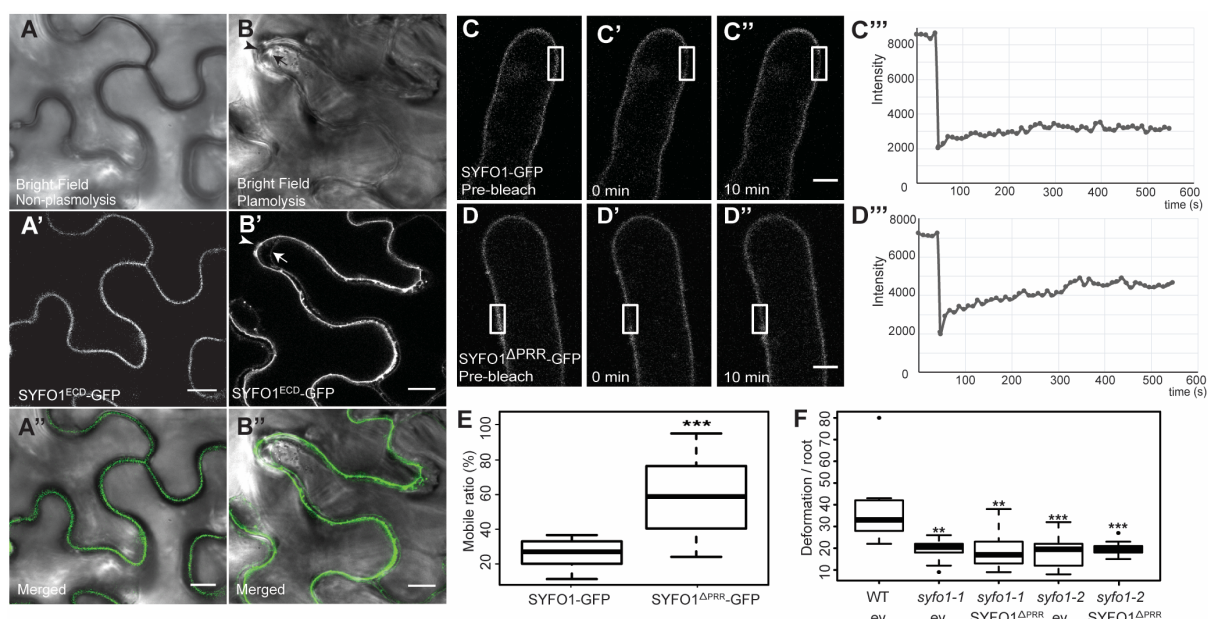
597
598
599
600
601
602
603
604
605
606
607
608

Figure 2. *syfo1* mutants are impaired in symbiotic root hair responses. Images show deformed root hairs (A), infection chambers (ICs) and infection threads (ITs) (B) on wild-type plants to illustrate the scored structures. Scale bars indicate 10 μ m. *syfo1* mutants show significantly reduced responsiveness to the presence of compatible rhizobia when assessing root hair deformations (C) and infection-related structures such as ICs + ITs (E). These phenotypes were complemented by introducing a genomic version of a full-length *SYFO1* gene driven by the endogenous *SYFO1* promoter (*syfo1-1c*, *syfo1-2c*) with an empty vector (ev) transformation control aside (D and F). Asterisks indicate a significant statistical difference based on a Tukey–Kramer multiple-comparison test with p-values <0.01 (**), <0.001 (***). Data are shown as mean \pm SE with independent 9-14 plants for phenotypical analysis, and 10 plants for complementation analysis.



609
610
611
612
613
614
615
616
617
618
619
620
621
622
623
624
625

Figure 3. SYFO1 functions as a symbiotic polarity factor in root hairs. SYFO1-GFP localizes homogeneously to the PM of root hairs under mock conditions (A). At 2 dpi with *S. meliloti*, SYFO1 transiently polarizes at subapical (B) and apical regions (C) of root hairs, before distributing equally along the PM during root hair deformation (D) and curling (E). The arrowhead marks cell wall autofluorescence around the IC (E and F). SYFO1 remains on the IT membrane (F and inset F'). Co-localisation between SYFO1-GFP and actin marker ABD2:mCherry (G-G'). The nucleus encircled with a dash line in G-G' is based on corresponding transmitted light image (not shown). The arrowheads point towards actin bundles orienting towards a nucleation centre at the apical shank of the root hair. Scale bars indicate 10 μ m. Protoplasts of a ROC expressing SYFO1 and counterstained with the styryl dye FM4-64 remain uniformly round at 0 dpi (H-H'') while focal membrane protrusions with accumulated SYFO1 were found at 5 hpi with Ds-Red expressing *S. meliloti* (I-I''). Scale bars indicate 5 μ m. (J) Quantification of membrane protrusions in protoplasts using different genetic backgrounds. Asterisks indicate a significant statistical difference based on an ANOVA followed by a Fisher LSD test, with p-values <0.05 (*), <0.01 (**). Data are shown as mean \pm SE of 3 independent biological replicates with n indicating the total number of protoplasts being scored.



626
627
628
629
630
631
632
633
634
635
636
637
638
639

Figure 4. Cell wall association of SYFO1 is essential for its function. The constitutively expressed ECD of SYFO1 labelled the cell periphery in non-plasmolysed cells (*A-A''*) and remained at the cell wall upon plasmolysis (*B-B''*). Arrowheads and arrows mark the cell wall and the retracted plasma membrane, respectively. FRAP experiments on roots hairs revealed a low mobility of full-length SYFO1 (*C-C''*) while deletion of the PRR resulted in an increased mobility of the protein (*D-D''*). Scale bars indicate 10 μ m. (*E*) Quantification of the mobile fractions of SYFO1 (n=17) and SYFO1^{ΔPRR} (n=12), asterisks indicate a significant statistical difference based on a student t test. (*F*) The SYFO1^{ΔPRR} variant failed to genetically complement both *syfo1* mutant alleles in comparison to roots transformed with the empty vector (ev) scoring n=10 independent root systems per genotype. Asterisks indicate a significant statistical difference based on a Tukey-Kramer multiple-comparison test with p-values <0.001 (***) , p<0.01 (**). Data are shown as mean \pm SE.